

LIBRARY
ROYAL AIRCRAFT ESTABLISHMENT
BEDFORD.



MINISTRY OF DEFENCE (PROCUREMENT EXECUTIVE)

AERONAUTICAL RESEARCH COUNCIL

REPORTS AND MEMORANDA

Some Calculations of Conditions at the Intersection of a Weak Shock Wave with a Strong Shock

BY I. MCGREGOR

Aerodynamics Dept., R.A.E., Bedford

LONDON: HER MAJESTY'S STATIONERY OFFICE

1973

PRICE 85p NET

Some Calculations of Conditions at the Intersection of a Weak Shock Wave with a Strong Shock

BY I. MCGREGOR

Aerodynamics Dept., R.A.E., Bedford

*Reports and Memoranda No. 3728**
March, 1972

Summary

Some comprehensive calculations of the flow conditions resulting from the intersection of a weak shock wave with a strong shock are presented and discussed, for a range of upstream Mach numbers between 1.4 and 2.8.

Such flows are of interest in connection with the sub-critical stability of air intakes, for example, and in the interaction of shock waves and boundary layers.

* Replaces R.A.E. Technical Report 72070—A.R.C. 34 013.

LIST OF CONTENTS

1. Introduction
2. Method of Calculation
3. Results and Discussion
4. Concluding Remarks

Symbols

References

Appendix. Oblique shock wave relations

Table 1

Illustrations—Figs. 1 to 5

Detachable Abstract Cards

1. Introduction

Several flows of practical interest involve the intersection of an oblique shock wave with a strong, nearly normal, shock. Two examples are shown in Fig. 1. The first is an air intake with a wedge compression surface, operating at a sub-critical mass flow ratio. If the vortex sheet originating from the intersection of the wedge shock and the terminal shock strikes or passes just inside the cowl lip, then unstable flow is likely to occur if the difference in total pressure on the two sides of the vortex sheet is greater than about 6 per cent.¹ The second example concerns the interaction between a boundary layer and a shock of strength sufficient to cause separation: an oblique shock is generated near the separation point which interacts with the incident shock wave.

The theory of shock intersections was developed a number of years ago,² and more recently the subject has been extensively studied by Henderson.^{3,4,5} However, few numerical values have been published, and it was to remedy this deficiency that the present calculations were undertaken. Although plane shocks are assumed, the results apply equally to the intersection of a conical shock with a strong axisymmetric shock. The flow at such an intersection is locally two-dimensional and identical to that for plane shocks with the same wave angles. Goldsmith and Griggs⁶ give a few examples of intersections of this type for intakes with conical centre bodies: although derived graphically, their results are in reasonable agreement with those given here.

2. Method of Calculation

Fig. 2 shows the notation used. A weak oblique shock, through which a deflection δ occurs, intersects a strong shock. The change in flow direction and Mach number below the intersection point, modifies the flow field behind the lower part of this shock. (To avoid confusion, this will be termed the 'rear' shock.) The flow direction and static pressure behind the rear shock must be the same as those behind the upper shock, but the Mach number and total pressure will be different. Consequently a surface of discontinuity (vortex sheet) separates the two flows downstream of the intersection: the inclination of this surface will be denoted by ε . The problem is to find the value of ε for given values of δ and the upstream Mach number M_1 , as once ε is known, the flow in the immediate vicinity of the intersection is completely determined.

Suppose for the moment that the surface of discontinuity is replaced by an infinitely thin lamina which is capable of supporting a pressure difference. This lamina may assume any angle between the limits ε_{\min} and ε_{\max} , given by

$$\varepsilon_{\min} = \delta - \delta_{\max}(M_2)$$

and

$$\varepsilon_{\max} = \delta_{\max}(M_1),$$

where $\delta_{\max}(M)$ is the maximum deflection through an oblique shock in a flow of Mach number M . The ratio of the static pressures p_3/p_4 on the two sides of the lamina, as its incidence is varied between these limits, is shown in Fig. 3 for an upstream Mach number of 2.4 and several values of δ ; it was assumed that the rear shock could be of either the strong or weak type. It is apparent that:

- (a) for each value of δ there is not more than one incidence for which $p_3/p_4 = 1$,
- (b) if $p_3/p_4 < 1$ at the minimum incidence ε_{\min} , then the condition $p_3/p_4 = 1$ can only be satisfied with a strong rear shock. Conversely, if $p_3/p_4 > 1$ at ε_{\min} , a weak shock is required.

Using these results, and the equations given in the Appendix for calculating the conditions behind an oblique shock, a computer program was constructed to find the value of ε by successive approximation.

3. Results and Discussion

The solutions are given in Table 1 for a range of M_1 between 1.4 and 2.8; δ was permitted to vary between 1 degree and the angle corresponding to $M_2 = 1$, in 1 degree steps. The table gives full details of the downstream flow; if the rear shock is of the weak type this is indicated by ** after the value of θ_4 . The value of p_3/p_4 corresponding to the computed value of ε is included as a check on the accuracy of the calculations. This ratio is normally within ± 0.0005 of unity except where the solution occurs very close to ε_{\min} —Fig. 3 shows such an example for $\delta = 8$ degrees. Although the value of ε should be correct to 0.01 degrees, in these circumstances, the extremely rapid rate of change of pressure with flow deflection behind the rear shock can lead to discrepancies of up to 0.005 in the value of p_3/p_4 , and there will be errors of a similar order in M_3 , P_3 and θ_3 .

The results are summarised in Fig. 4. For flows of the type assumed, i.e. with a strong upper shock, there is a limiting value of δ for which solutions could be found. This occurs when $\varepsilon = \varepsilon_{\max}$ and the flow deflection through the upper shock is a maximum. It is somewhat below the boundary given by Henderson⁵ for a general 3-shock confluence, and to extend the present solutions to higher values of δ , a weak upper shock would be required. The lowest Mach number for which an intersection with a strong upper shock can exist appears to be about 1.33. If M_1 is less than 2.2, the rear shock is always of the strong type, and if M_1 is less than 2.4, M_3 is always subsonic. If M_1 is greater than 2.4, M_3 may be subsonic or supersonic, depending on the value of δ .

When M_1 is greater than about 1.5*, the solutions for the lower values of δ require the angle of the upper shock, θ_4 , to be greater than 90 degrees. If the flow behind the shock were supersonic this could only represent an incident wave originating from a point upstream of the intersection. However, the actual flow behind the shock is subsonic, so that its shape is determined by the whole of the downstream flow field. Although this possibility was discounted in Ref. 6, there does not appear to be any fundamental reason why locally the shock should not have an inclination greater than 90 degrees, if this is necessary to give the correct flow direction and pressure immediately downstream of the intersection point.

The changes in the shock patterns as δ is increased are illustrated in Fig. 5 for an upstream Mach number of 1.6. For small values of δ the surface of discontinuity is inclined downwards, but when a certain point is reached ($\delta \simeq 4$ degrees in this case), $\varepsilon = 0$ and the upper shock is normal—the well-known stationary Mach reflection. When $\delta \simeq 8.5$ degrees, ε has become equal to δ and the rear shock is normal. With further increase in δ , ε exceeds δ and the rear shock is inclined forwards. As the downstream flow is subsonic, this would again appear to represent a physically possible configuration. (The supersonic values of M_3 , found when M_1 is greater than 2.4, only occur when ε is less than δ , that is, with a rearwardly inclined shock.)

4. Concluding Remarks

It should be emphasised that the results presented strictly only refer to conditions at, or very close to, the intersection point. The inclination of the upper shock at this point is determined by the upstream Mach number and the deflection through the forward shock. If this inclination is not compatible with that of the upper shock in the absence of the forward shock, then the upper shock must bend locally to match the value required at the intersection point, and this alteration in shock shape will modify the flow downstream. However, if the change in inclination is reasonably small—perhaps up to 15 degrees for an initially near-normal shock—the results should give a reasonably accurate picture of the actual flow field some distance downstream of the intersection.

* To be precise, greater than $\sqrt{(\gamma + 3)/2} = 1.483$, for vanishingly small values of δ (Ref. 2).

LIST OF SYMBOLS

M	Mach number
p	Static pressure
P	Total pressure
θ	Angle of shock wave
δ	Flow deflection through the weak shock wave
ε	Inclination of surface of discontinuity
γ	Ratio of specific heats (taken as 1.4 for air)

Suffices

1-4	Regions of the flow defined in Fig. 2
max	Maximum value
min	Minimum value

REFERENCES

- | <i>No.</i> | <i>Author(s)</i> | <i>Title, etc.</i> |
|------------|---|---|
| 1 | S. A. Fisher, M. C. Neale and
A. J. Brooks | On the sub-critical stability of variable ramp intakes at Mach numbers around 2.
A.R.C. R. & M. 3711 (1970). |
| 2 | R. Courant and K. O. Friedrichs .. | <i>Supersonic flow and shock waves.</i>
Interscience Publishers Inc., New York, pp. 331–350 (1948). |
| 3 | L. F. Henderson | On the confluence of three shock waves in a perfect gas.
<i>Aero Quarterly</i> , Vol. XV, p. 181 (1964). |
| 4 | L. F. Henderson | The three-shock confluence on a simple wedge intake.
<i>Aero Quarterly</i> , Vol. XVI, p. 42 (1965). |
| 5 | L. F. Henderson | On a class of multi-shock interactions in a perfect gas.
<i>Aero Quarterly</i> , Vol. XVII, p. 1 (1966). |
| 6 | E. L. Goldsmith and C. F. Griggs .. | The estimation of shock pressure recovery and external drag of conical centre-body intakes at supersonic speeds.
A.R.C. R. & M. 3035 (1953). |
| 7 | Ames Research Staff | Equations, tables and charts for compressible flow.
NACA Report 1135 (1953). |
| 8 | V. R. Mascitti | A closed form solution to oblique shock wave properties
<i>Journal of Aircraft</i> , Vol. 6, No. 1 (1969). |

APPENDIX

Oblique Shock Wave Relations

The angle θ of an oblique shock generated by deflecting a supersonic stream (Mach number M_1) through an angle δ is governed by the equation⁷

$$\sin^6 \theta + b \sin^4 \theta + c \sin^2 \theta + d = 0,$$

where

$$b = -(M_1^2 + 2)/M_1^2 - \gamma \sin^2 \delta,$$

$$c = (2M_1^2 + 1)/M_1^4 + [(\gamma + 1)^2/4 + (\gamma - 1)] \sin^2 \delta$$

and

$$d = -\cos^2 \delta / M_1^4.$$

This is a cubic in $\sin^2 \theta$, whose solutions are given by⁸

$$\sin^2 \theta = -b/3 + \frac{2}{3}(b^2 - 3c)^{\frac{1}{2}} \cos [(\phi + n\pi)/3],$$

where

$$\cos \phi = (\frac{2}{3}bc - b^3 - \frac{27}{2}d)/(b^2 - 3c)^{\frac{3}{2}}$$

and $n = 0$ corresponds to the 'strong' shock solution,
 $n = 4$ corresponds to the 'weak' shock solution, and
 $n = 2$ results in a non-physical solution with a decrease in entropy.

The ratio of static and total pressures across the shock, and the Mach number downstream of it, are given by⁷

$$p_2/p_1 = [2\gamma m - (\gamma - 1)]/(\gamma + 1),$$

$$P_2/P_1 = \left[\frac{(\gamma + 1)m}{(\gamma - 1)m + 2} \right]^{\frac{\gamma}{\gamma - 1}} \left(\frac{p_2}{p_1} \right)^{-\frac{1}{\gamma - 1}},$$

and

$$M_2 = \left\{ \frac{(\gamma + 1)^2 M_1^2 m - 4(m - 1)(\gamma m + 1)}{[2\gamma m - (\gamma - 1)][(\gamma - 1)m + 2]} \right\}^{\frac{1}{2}}$$

where $m = M_1^2 \sin^2 \theta$.

Two further relations are required. The first is

$$\frac{1}{M_1^2} = \sin^2 \theta - \frac{\gamma + 1}{2} \frac{\tan \theta}{\tan \theta + \cot \delta}$$

which may be rearranged as

$$\delta = \tan^{-1} \left[\tan \theta \left\{ \frac{\gamma + 1}{2} \frac{M_1^2}{M_1^2 \sin^2 \theta - 1} - 1 \right\} \right]^{-1}$$

and the second gives the shock wave angle for maximum stream deflection behind the shock

$$\sin^2 \theta_{\max} = \frac{1}{4\gamma M_1^2} \{ (\gamma + 1)M_1^2 - 4 + [(\gamma + 1)\{(\gamma + 1)M_1^4 + 8(\gamma - 1)M_1^2 + 16\}]^{\frac{1}{2}} \},$$

from which δ_{\max} can be determined.

TABLE 1

Flow Conditions at the Intersection of a Weak Shock Wave and a Strong Shock

M_1	δ	ε	p_3/p_4	p_4/p_1	M_3	M_4	P_3/P_4	P_4/P_1	θ_3	θ_4
1.4	1.0	6.10	1.000	2.055	0.785	0.778	1.007	0.963	97.8	80.3
1.4	2.0	7.54	1.000	2.007	0.818	0.806	1.012	0.967	99.1	77.1
1.4	3.0	8.79	1.000	1.928	0.864	0.850	1.015	0.972	101.4	73.2
1.5	1.0	0.55	1.000	2.458	0.714	0.701	1.011	0.930	88.4	89.4
1.5	2.0	2.09	1.000	2.454	0.727	0.704	1.021	0.930	88.1	87.6
1.5	3.0	3.72	1.000	2.443	0.741	0.710	1.030	0.931	88.1	85.6
1.5	4.0	5.44	1.000	2.424	0.759	0.720	1.036	0.933	88.3	83.4
1.5	5.0	7.24	1.000	2.393	0.780	0.738	1.041	0.936	89.1	80.9
1.5	6.0	9.07	1.000	2.343	0.808	0.765	1.043	0.940	90.5	77.9
1.5	7.0	10.80	1.000	2.259	0.848	0.810	1.040	0.947	93.0	74.0
1.6	1.0	— 4.46	1.000	2.802	0.695	0.678	1.015	0.897	83.2	94.4
1.6	2.0	— 3.06	1.000	2.812	0.705	0.673	1.029	0.896	82.3	93.0
1.6	3.0	— 1.56	1.000	2.818	0.715	0.670	1.041	0.895	81.5	91.5
1.6	4.0	0.04	1.000	2.820	0.725	0.668	1.052	0.895	80.9	90.0
1.6	5.0	1.74	1.000	2.817	0.736	0.670	1.061	0.895	80.5	88.3
1.6	6.0	3.54	1.000	2.809	0.748	0.674	1.069	0.896	80.3	86.5
1.6	7.0	5.45	1.000	2.793	0.761	0.683	1.074	0.898	80.5	84.6
1.6	8.0	7.45	1.000	2.767	0.777	0.697	1.077	0.900	81.0	82.3
1.6	9.0	9.55	1.000	2.725	0.796	0.719	1.077	0.905	82.1	79.7
1.6	10.0	11.69	1.000	2.656	0.825	0.754	1.072	0.911	84.2	76.5
1.6	11.0	13.69	1.000	2.533	0.872	0.816	1.060	0.923	87.9	72.0
1.7	1.0	— 8.72	1.000	3.144	0.693	0.672	1.019	0.862	79.7	97.7
1.7	2.0	— 7.43	1.000	3.162	0.704	0.663	1.036	0.860	78.5	96.5
1.7	3.0	— 6.04	1.000	3.177	0.714	0.655	1.053	0.859	77.4	95.2
1.7	4.0	— 4.56	1.000	3.190	0.723	0.649	1.068	0.857	76.3	93.9
1.7	5.0	— 2.98	1.000	3.199	0.732	0.644	1.081	0.856	75.4	92.5
1.7	6.0	— 1.32	1.000	3.204	0.741	0.641	1.092	0.856	74.7	91.1
1.7	7.0	0.45	1.000	3.205	0.750	0.641	1.102	0.856	74.1	89.6
1.7	8.0	2.31	1.000	3.201	0.759	0.643	1.110	0.856	73.6	88.1
1.7	9.0	4.27	1.000	3.192	0.768	0.648	1.115	0.857	73.5	86.4
1.7	10.0	6.34	1.000	3.174	0.778	0.656	1.117	0.859	73.6	84.5
1.7	11.0	8.52	1.000	3.147	0.790	0.671	1.117	0.862	74.2	82.4
1.7	12.0	10.82	1.000	3.103	0.806	0.693	1.112	0.866	75.4	80.0
1.7	13.0	13.22	1.000	3.031	0.828	0.728	1.102	0.874	77.6	76.9
1.7	14.0	15.59	1.000	2.901	0.868	0.790	1.083	0.887	81.5	72.5
1.8	1.0	— 12.33	1.000	3.497	0.700	0.674	1.023	0.825	77.2	100.1
1.8	2.0	— 11.12	1.000	3.523	0.711	0.661	1.045	0.822	75.8	98.9
1.8	3.0	— 9.81	1.000	3.545	0.722	0.650	1.065	0.820	74.4	97.7
1.8	4.0	— 8.42	1.000	3.565	0.733	0.641	1.084	0.818	73.1	96.5
1.8	5.0	— 6.94	1.000	3.582	0.743	0.632	1.102	0.816	71.9	95.3
1.8	6.0	— 5.36	1.000	3.595	0.752	0.626	1.117	0.815	70.8	94.0
1.8	7.0	— 3.70	1.000	3.605	0.760	0.621	1.131	0.814	69.8	92.7
1.8	8.0	— 1.96	1.000	3.611	0.768	0.618	1.142	0.813	69.0	91.4
1.8	9.0	— 0.13	1.000	3.613	0.775	0.617	1.151	0.813	68.3	90.1
1.8	10.0	1.79	1.000	3.611	0.782	0.618	1.158	0.813	67.8	88.7
1.8	11.0	3.81	1.000	3.604	0.789	0.621	1.162	0.814	67.5	87.2
1.8	12.0	5.93	1.000	3.590	0.795	0.628	1.163	0.815	67.4	85.5

TABLE 1—continued

M_1	δ	ε	p_3/p_4	p_4/p_1	M_3	M_4	P_3/P_4	P_4/P_1	θ_3	θ_4
1.8	13.0	8.17	1.000	3.568	0.803	0.639	1.161	0.817	67.8	83.7
1.8	14.0	10.53	1.000	3.534	0.812	0.656	1.155	0.821	68.6	81.6
1.8	15.0	13.02	1.000	3.479	0.824	0.682	1.144	0.827	70.2	79.1
1.8	16.0	15.65	1.000	3.388	0.845	0.725	1.125	0.837	72.9	75.9
1.8	17.0	18.21	1.000	3.206	0.890	0.806	1.091	0.856	78.3	70.8
1.9	1.0	-15.41	1.000	3.867	0.710	0.679	1.027	0.786	75.3	101.9
1.9	2.0	-14.26	1.000	3.900	0.723	0.664	1.054	0.782	73.7	100.7
1.9	3.0	-13.02	1.000	3.930	0.736	0.650	1.079	0.779	72.2	99.5
1.9	4.0	-11.67	1.000	3.956	0.748	0.638	1.102	0.777	70.7	98.3
1.9	5.0	-10.25	1.000	3.979	0.759	0.627	1.124	0.774	69.3	97.2
1.9	6.0	-8.74	1.000	3.999	0.770	0.618	1.144	0.772	68.0	96.0
1.9	7.0	-7.14	1.000	4.015	0.779	0.610	1.161	0.770	66.8	94.8
1.9	8.0	-5.47	1.000	4.028	0.787	0.604	1.177	0.769	65.6	93.7
1.9	9.0	-3.74	1.000	4.037	0.795	0.599	1.190	0.768	64.6	92.5
1.9	10.0	-1.90	1.000	4.043	0.801	0.597	1.200	0.768	63.7	91.3
1.9	11.0	0.00	1.000	4.045	0.807	0.596	1.208	0.767	63.0	90.0
1.9	12.0	1.99	1.000	4.043	0.812	0.597	1.213	0.768	62.5	88.7
1.9	13.0	4.06	1.000	4.036	0.816	0.600	1.215	0.768	62.1	87.3
1.9	14.0	6.22	1.000	4.022	0.820	0.607	1.213	0.770	62.0	85.8
1.9	15.0	8.49	1.000	4.002	0.824	0.617	1.208	0.772	62.2	84.2
1.9	16.0	10.90	1.000	3.969	0.828	0.632	1.199	0.775	63.0	82.3
1.9	17.0	13.45	1.000	3.920	0.835	0.655	1.184	0.780	64.3	80.1
1.9	18.0	16.17	1.000	3.840	0.847	0.691	1.162	0.789	66.7	77.3
1.9	19.0	19.04	1.000	3.691	0.874	0.756	1.127	0.804	71.0	73.1
2.0	1.0	-18.06	1.000	4.256	0.722	0.686	1.032	0.746	73.8	103.2
2.0	2.0	-16.96	1.000	4.298	0.737	0.669	1.063	0.741	72.1	102.0
2.0	3.0	-15.75	1.000	4.335	0.752	0.653	1.093	0.738	70.4	100.8
2.0	4.0	-14.45	1.000	4.368	0.766	0.638	1.121	0.734	68.8	99.7
2.0	5.0	-13.07	1.000	4.396	0.779	0.625	1.148	0.731	67.2	98.6
2.0	6.0	-11.58	1.000	4.422	0.791	0.614	1.172	0.729	65.8	97.4
2.0	7.0	-10.04	1.000	4.443	0.802	0.604	1.195	0.727	64.4	96.3
2.0	8.0	-8.42	1.000	4.461	0.813	0.596	1.215	0.725	63.0	95.2
2.0	9.0	-6.73	1.000	4.476	0.821	0.589	1.232	0.723	61.8	94.1
2.0	10.0	-4.96	1.000	4.487	0.829	0.583	1.246	0.722	60.7	93.0
2.0	11.0	-3.13	1.000	4.495	0.835	0.580	1.257	0.721	59.7	91.9
2.0	12.0	-1.23	1.000	4.499	0.840	0.578	1.266	0.721	58.8	90.7
2.0	13.0	0.74	1.000	4.500	0.844	0.577	1.271	0.721	58.1	89.6
2.0	14.0	2.79	1.000	4.496	0.846	0.579	1.273	0.721	57.6	88.3
2.0	15.0	4.91	1.000	4.487	0.848	0.583	1.271	0.722	57.2	87.0
2.0	16.0	7.13	1.000	4.473	0.849	0.590	1.266	0.724	57.2	85.6
2.0	17.0	9.45	1.000	4.450	0.850	0.601	1.256	0.726	57.4	84.1
2.0	18.0	11.89	1.000	4.417	0.850	0.616	1.242	0.729	58.1	82.3
2.0	19.0	14.51	1.000	4.366	0.852	0.639	1.222	0.734	59.5	80.3
2.0	20.0	17.30	1.000	4.286	0.859	0.674	1.194	0.743	61.8	77.6
2.0	21.0	20.32	1.000	4.136	0.878	0.736	1.151	0.758	66.3	73.8
2.1	1.0	-20.37	1.000	4.667	0.734	0.694	1.037	0.704	72.6	104.2
2.1	2.0	-19.30	1.000	4.716	0.752	0.674	1.074	0.699	70.8	103.0
2.1	3.0	-18.12	1.000	4.761	0.770	0.656	1.109	0.695	69.0	101.9
2.1	4.0	-16.84	1.000	4.801	0.786	0.639	1.142	0.691	67.3	100.7
2.1	5.0	-15.49	1.000	4.836	0.802	0.625	1.174	0.688	65.6	99.6

TABLE 1—continued

M_1	δ	ε	p_3/p_4	p_4/p_1	M_3	M_4	P_3/P_4	P_4/P_1	θ_3	θ_4
2.1	6.0	-14.03	1.000	4.866	0.816	0.611	1.204	0.685	63.9	98.5
2.1	7.0	-12.50	1.000	4.893	0.829	0.600	1.231	0.682	62.4	97.4
2.1	8.0	-10.89	1.000	4.916	0.841	0.590	1.255	0.680	60.9	96.3
2.1	9.0	- 9.22	1.000	4.935	0.851	0.581	1.277	0.678	59.5	95.3
2.1	10.0	- 7.49	1.000	4.950	0.859	0.574	1.295	0.677	58.3	94.2
2.1	11.0	- 5.70	1.000	4.962	0.867	0.569	1.311	0.676	57.1	93.2
2.1	12.0	- 3.85	1.000	4.971	0.872	0.565	1.322	0.675	56.0	92.1
2.1	13.0	- 1.94	1.000	4.977	0.876	0.562	1.331	0.674	55.1	91.1
2.1	14.0	0.03	1.000	4.978	0.879	0.561	1.336	0.674	54.2	90.0
2.1	15.0	2.05	1.000	4.976	0.881	0.562	1.337	0.674	53.6	88.9
2.1	16.0	4.15	1.000	4.970	0.881	0.565	1.334	0.675	53.1	87.7
2.1	17.0	6.32	1.000	4.959	0.880	0.570	1.327	0.676	52.9	86.5
2.1	18.0	8.59	1.000	4.941	0.878	0.578	1.316	0.678	52.9	85.1
2.1	19.0	10.96	1.000	4.915	0.875	0.590	1.301	0.680	53.2	83.6
2.1	20.0	13.46	1.000	4.877	0.872	0.607	1.281	0.684	54.1	81.9
2.1	21.0	16.13	1.000	4.820	0.871	0.631	1.253	0.689	55.6	79.9
2.1	22.0	19.03	1.000	4.728	0.873	0.670	1.217	0.698	58.3	77.2
2.1	23.0	22.20	1.000	4.548	0.889	0.741	1.161	0.716	63.5	73.2
2.2	1.0	-22.39	1.000	5.099	0.748	0.702	1.043	0.663	71.7	105.1
2.2	2.0	-21.34	1.000	5.158	0.768	0.680	1.084	0.657	69.8	103.8
2.2	3.0	-20.17	1.000	5.211	0.788	0.659	1.125	0.652	67.9	102.6
2.2	4.0	-18.92	1.000	5.257	0.808	0.641	1.165	0.648	66.0	101.5
2.2	5.0	-17.56	1.000	5.298	0.825	0.625	1.202	0.644	64.2	100.3
2.2	6.0	-16.11	1.000	5.334	0.842	0.610	1.237	0.641	62.4	99.2
2.2	7.0	-14.58	1.000	5.366	0.857	0.597	1.270	0.638	60.8	98.2
2.2	8.0	-12.98	1.000	5.393	0.870	0.585	1.300	0.636	59.2	97.1
2.2	9.0	-11.32	1.000	5.416	0.882	0.575	1.326	0.634	57.7	96.1
2.2	10.0	- 9.60	1.000	5.435	0.892	0.567	1.349	0.632	56.3	95.1
2.2	11.0	- 7.83	1.000	5.451	0.901	0.560	1.368	0.631	54.9	94.1
2.2	12.0	- 6.01	1.002	5.463	0.905	0.555	1.383	0.630	53.8	93.1
2.2	13.0	- 4.14	1.004	5.472	0.908	0.551	1.394	0.629	52.8	92.1
2.2	14.0	- 2.22	1.004	5.478	0.912	0.548	1.402	0.628	51.8	91.1
2.2	15.0	- 0.25	1.003	5.480	0.915	0.547	1.406	0.628	50.9	90.1
2.2	16.0	1.77	1.003	5.479	0.915	0.548	1.406	0.628	50.2	89.1
2.2	17.0	3.85	1.004	5.473	0.912	0.550	1.401	0.629	49.7	88.0
2.2	18.0	5.99	1.003	5.463	0.910	0.554	1.392	0.630	49.3	86.9
2.2	19.0	8.21	1.001	5.448	0.909	0.561	1.380	0.631	49.0	85.7
2.2	20.0	10.52	1.000	5.426	0.904	0.571	1.362	0.633	49.1	84.4
2.2	21.0	12.95	1.000	5.394	0.898	0.585	1.339	0.636	49.7	82.9
2.2	22.0	15.52	1.000	5.347	0.892	0.604	1.310	0.640	50.8	81.2
2.2	23.0	18.29	1.000	5.277	0.887	0.633	1.274	0.646	52.7	79.1
2.2	24.0	21.33	1.000	5.158	0.887	0.680	1.225	0.657	56.1	76.2
2.2	25.0	24.72	1.000	4.890	0.909	0.779	1.145	0.683	63.4	71.1
2.3	1.0	-24.16	1.000	5.553	0.760	0.710	1.048	0.622	70.9	105.7
2.3	2.0	-23.12	1.000	5.622	0.783	0.685	1.096	0.616	68.9	104.4
2.3	3.0	-21.99	1.000	5.682	0.807	0.663	1.143	0.610	66.8	103.2
2.3	4.0	-20.72	1.000	5.737	0.829	0.643	1.189	0.606	64.9	102.0
2.3	5.0	-19.36	1.000	5.785	0.849	0.625	1.232	0.602	63.0	100.9
2.3	6.0	-17.90	1.000	5.826	0.868	0.608	1.273	0.598	61.1	99.8
2.3	7.0	-16.37	1.000	5.863	0.886	0.594	1.312	0.595	59.4	98.7
2.3	8.0	-14.76	1.000	5.894	0.901	0.581	1.347	0.592	57.7	97.7

TABLE 1—continued

M_1	δ	ε	p_3/p_4	p_4/p_1	M_3	M_4	P_3/P_4	P_4/P_1	θ_3	θ_4
2.3	9.0	-13.10	1.003	5.921	0.910	0.570	1.377	0.590	56.3	96.7
2.3	10.0	-11.38	0.996	5.944	0.931	0.561	1.409	0.588	54.3	95.7**
2.3	11.0	- 9.62	0.999	5.962	0.938	0.553	1.431	0.587	53.0	94.8**
2.3	12.0	- 7.81	1.000	5.977	0.945	0.546	1.450	0.586	51.8	93.8**
2.3	13.0	- 5.96	1.000	5.989	0.951	0.541	1.466	0.585	50.5	92.9**
2.3	14.0	- 4.07	1.000	5.998	0.955	0.538	1.476	0.584	49.4	92.0**
2.3	15.0	- 2.14	1.000	6.003	0.957	0.535	1.483	0.583	48.4	91.0**
2.3	16.0	- 0.17	1.000	6.005	0.958	0.534	1.484	0.583	47.5	90.1**
2.3	17.0	1.84	1.000	6.004	0.956	0.535	1.481	0.583	46.7	89.1**
2.3	18.0	3.91	1.000	5.998	0.953	0.537	1.474	0.584	46.1	88.1**
2.3	19.0	6.03	1.000	5.989	0.949	0.541	1.462	0.585	45.7	87.1**
2.3	20.0	8.22	1.000	5.974	0.943	0.548	1.446	0.586	45.5	86.0**
2.3	21.0	10.50	0.998	5.953	0.937	0.556	1.425	0.588	45.4	84.8**
2.3	22.0	12.86	1.003	5.924	0.923	0.569	1.398	0.590	46.1	83.4
2.3	23.0	15.36	1.000	5.883	0.917	0.585	1.366	0.593	46.8	81.9
2.3	24.0	18.03	1.000	5.823	0.907	0.610	1.327	0.598	48.3	80.1
2.3	25.0	20.95	1.000	5.728	0.900	0.646	1.277	0.607	50.9	77.8
2.3	26.0	24.24	1.000	5.547	0.901	0.712	1.208	0.622	56.0	74.2
2.4	1.0	-25.74	1.000	6.029	0.774	0.718	1.054	0.581	70.3	106.2
2.4	2.0	-24.73	1.000	6.108	0.801	0.691	1.108	0.575	68.1	104.9
2.4	3.0	-23.57	1.000	6.178	0.826	0.667	1.162	0.569	66.0	103.7
2.4	4.0	-22.30	1.000	6.241	0.851	0.644	1.214	0.564	63.9	102.5
2.4	5.0	-20.92	1.000	6.295	0.874	0.624	1.264	0.560	61.9	101.3
2.4	6.0	-19.45	1.000	6.343	0.895	0.607	1.312	0.556	60.0	100.2
2.4	7.0	-17.90	1.002	6.384	0.912	0.591	1.355	0.553	58.3	99.1
2.4	8.0	-16.28	0.996	6.420	0.937	0.577	1.401	0.550	56.2	98.1**
2.4	9.0	-14.61	1.000	6.450	0.949	0.565	1.436	0.548	54.7	97.1**
2.4	10.0	-12.89	1.000	6.476	0.962	0.555	1.469	0.546	53.1	96.2**
2.4	11.0	-11.13	1.000	6.497	0.973	0.546	1.498	0.544	51.5	95.2**
2.4	12.0	- 9.32	1.000	6.515	0.983	0.539	1.522	0.543	50.1	94.3**
2.4	13.0	- 7.48	1.000	6.529	0.990	0.533	1.541	0.542	48.8	93.4**
2.4	14.0	- 5.61	1.000	6.540	0.995	0.529	1.555	0.541	47.5	92.6**
2.4	15.0	- 3.70	1.000	6.548	0.998	0.526	1.564	0.541	46.4	91.7**
2.4	16.0	- 1.76	1.000	6.552	0.999	0.524	1.568	0.540	45.4	90.8**
2.4	17.0	0.21	1.000	6.553	0.998	0.523	1.567	0.540	44.5	89.9**
2.4	18.0	2.23	1.000	6.551	0.995	0.524	1.561	0.540	43.7	89.0**
2.4	19.0	4.29	1.000	6.546	0.990	0.526	1.550	0.541	43.1	88.1**
2.4	20.0	6.39	1.000	6.536	0.984	0.530	1.533	0.541	42.6	87.1**
2.4	21.0	8.56	1.000	6.521	0.975	0.536	1.513	0.543	42.4	86.0**
2.4	22.0	10.79	1.000	6.501	0.966	0.545	1.487	0.544	42.4	84.9**
2.4	23.0	13.12	1.000	6.472	0.955	0.556	1.456	0.546	42.7	83.7**
2.4	24.0	15.57	0.999	6.433	0.943	0.572	1.420	0.549	43.3	82.3**
2.4	25.0	18.18	1.003	6.377	0.926	0.594	1.376	0.554	44.9	80.7
2.4	26.0	21.00	1.000	6.292	0.917	0.625	1.323	0.560	46.9	78.6
2.4	27.0	24.17	1.000	6.143	0.909	0.679	1.255	0.572	51.0	75.7
2.4	28.0	27.84	1.000	5.749	0.930	0.809	1.136	0.605	60.8	69.8
2.5	1.0	-27.12	1.000	6.529	0.786	0.725	1.060	0.542	69.7	106.6
2.5	2.0	-26.13	1.000	6.617	0.816	0.696	1.121	0.535	67.5	105.3
2.5	3.0	-24.97	1.000	6.698	0.845	0.669	1.181	0.529	65.3	104.0
2.5	4.0	-23.68	1.000	6.769	0.872	0.645	1.240	0.524	63.1	102.8
2.5	5.0	-22.29	1.000	6.830	0.898	0.624	1.298	0.520	61.0	101.6

TABLE 1—continued

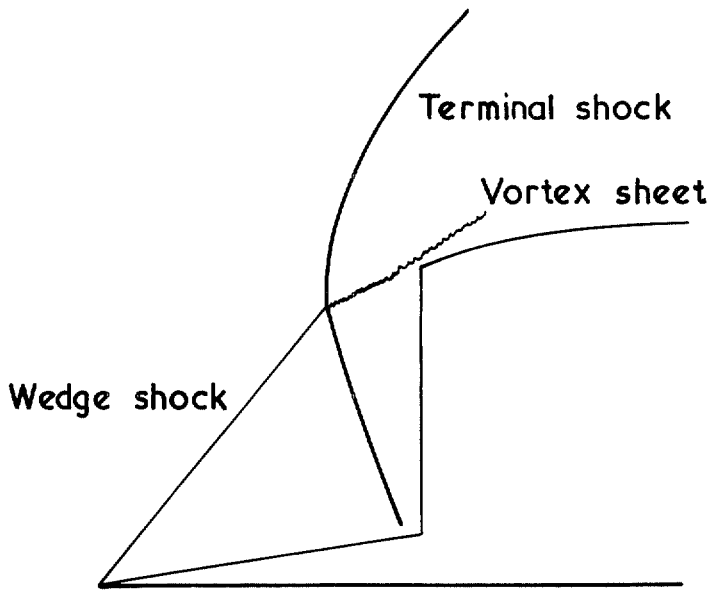
M_1	δ	ϵ	P_3/P_4	P_4/P_1	M_3	M_4	P_3/P_4	P_4/P_1	θ_3	θ_4
2.5	6.0	-20.79	1.003	6.884	0.918	0.605	1.350	0.516	59.2	100.5
2.5	7.0	-19.23	0.998	6.930	0.948	0.588	1.407	0.513	57.0	99.4**
2.5	8.0	-17.60	1.000	6.969	0.964	0.574	1.453	0.510	55.2	98.4**
2.5	9.0	-15.91	1.000	7.003	0.982	0.561	1.497	0.507	53.4	97.4**
2.5	10.0	-14.17	1.000	7.032	0.997	0.550	1.537	0.505	51.8	96.5**
2.5	11.0	-12.40	1.000	7.056	1.010	0.541	1.571	0.504	50.1	95.6**
2.5	12.0	-10.59	1.000	7.076	1.021	0.533	1.600	0.502	48.6	94.7**
2.5	13.0	- 8.75	1.000	7.092	1.029	0.526	1.623	0.501	47.2	93.8**
2.5	14.0	- 6.88	1.000	7.105	1.036	0.521	1.641	0.500	45.9	93.0**
2.5	15.0	- 4.99	1.000	7.115	1.039	0.517	1.652	0.500	44.7	92.2**
2.5	16.0	- 3.07	1.000	7.121	1.041	0.515	1.658	0.499	43.5	91.3**
2.5	17.0	- 1.12	1.000	7.124	1.040	0.513	1.659	0.499	42.5	90.5**
2.5	18.0	0.85	1.000	7.125	1.038	0.513	1.653	0.499	41.6	89.6**
2.5	19.0	2.86	1.000	7.122	1.033	0.514	1.643	0.499	40.9	88.8**
2.5	20.0	4.91	1.000	7.115	1.026	0.517	1.627	0.500	40.3	87.9**
2.5	21.0	7.00	1.000	7.104	1.018	0.521	1.606	0.500	39.8	87.0**
2.5	22.0	9.15	1.000	7.089	1.007	0.527	1.579	0.501	39.6	86.0**
2.5	23.0	11.36	1.000	7.068	0.995	0.536	1.548	0.503	39.5	84.9**
2.5	24.0	13.66	1.000	7.039	0.982	0.547	1.512	0.505	39.8	83.8**
2.5	25.0	16.07	1.000	7.000	0.967	0.562	1.470	0.508	40.5	82.5**
2.5	26.0	18.62	1.000	6.945	0.951	0.583	1.421	0.512	41.7	81.0**
2.5	27.0	21.39	1.003	6.863	0.931	0.612	1.363	0.517	44.0	79.1
2.5	28.0	24.49	1.000	6.726	0.920	0.660	1.291	0.527	47.4	76.5
2.5	29.0	28.14	1.000	6.405	0.923	0.763	1.180	0.551	55.4	71.7
2.6	1.0	-28.39	1.000	7.047	0.799	0.732	1.067	0.504	69.2	107.0
2.6	2.0	-27.38	1.000	7.151	0.832	0.700	1.134	0.497	66.9	105.6
2.6	3.0	-26.21	1.000	7.242	0.863	0.672	1.202	0.491	64.6	104.3
2.6	4.0	-24.90	1.000	7.321	0.893	0.646	1.269	0.486	62.4	103.0
2.6	5.0	-23.48	1.002	7.390	0.919	0.623	1.332	0.481	60.4	101.8
2.6	6.0	-21.97	0.998	7.449	0.953	0.603	1.399	0.477	58.0	100.7**
2.6	7.0	-20.38	1.000	7.500	0.974	0.585	1.456	0.474	56.1	99.6**
2.6	8.0	-18.72	1.000	7.544	0.996	0.570	1.512	0.471	54.2	98.6**
2.6	9.0	-17.01	1.000	7.581	1.016	0.557	1.563	0.469	52.3	97.6**
2.6	10.0	-15.26	1.000	7.612	1.033	0.545	1.609	0.467	50.6	96.7**
2.6	11.0	-13.47	1.000	7.639	1.048	0.535	1.649	0.465	48.9	95.8**
2.6	12.0	-11.65	1.000	7.661	1.060	0.527	1.683	0.464	47.3	95.0**
2.6	13.0	- 9.81	1.000	7.679	1.070	0.520	1.711	0.463	45.8	94.1**
2.6	14.0	- 7.95	1.000	7.694	1.077	0.514	1.732	0.462	44.4	93.3**
2.6	15.0	- 6.05	1.000	7.705	1.082	0.510	1.747	0.461	43.1	92.5**
2.6	16.0	- 4.14	0.999	7.713	1.084	0.507	1.756	0.461	41.9	91.7**
2.6	17.0	- 2.22	0.999	7.718	1.084	0.505	1.758	0.460	40.8	90.9**
2.6	18.0	- 0.27	0.999	7.720	1.081	0.504	1.753	0.460	39.8	90.1**
2.6	19.0	1.71	0.999	7.719	1.077	0.504	1.743	0.460	39.0	89.3**
2.6	20.0	3.71	0.999	7.714	1.070	0.506	1.726	0.460	38.2	88.5**
2.6	21.0	5.75	1.000	7.707	1.061	0.509	1.704	0.461	37.6	87.6**
2.6	22.0	7.82	1.000	7.695	1.050	0.514	1.677	0.462	37.2	86.7**
2.6	23.0	9.95	1.000	7.678	1.037	0.520	1.644	0.463	37.0	85.8**
2.6	24.0	12.15	1.000	7.655	1.023	0.529	1.607	0.464	37.0	84.8**
2.6	25.0	14.42	1.000	7.625	1.007	0.540	1.564	0.466	37.3	83.7**
2.6	26.0	16.80	1.000	7.585	0.989	0.555	1.516	0.469	37.9	82.5**
2.6	27.0	19.33	1.000	7.529	0.970	0.575	1.461	0.472	39.1	81.0**

TABLE 1—continued

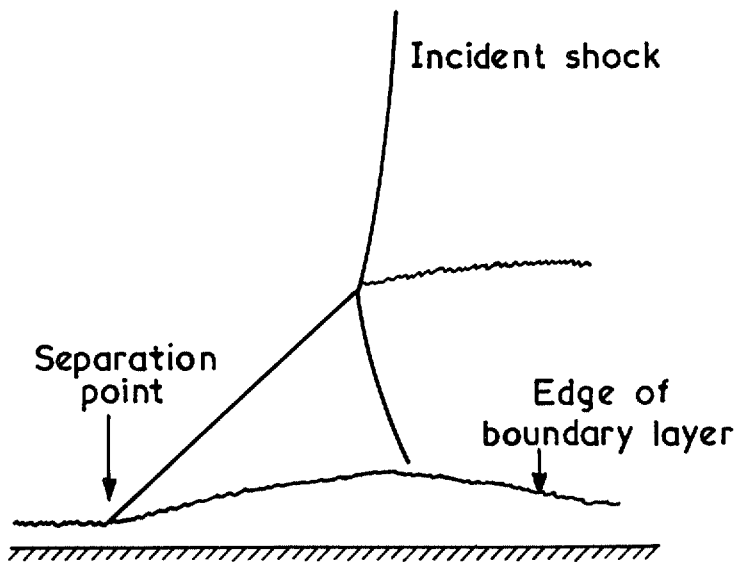
M_1	δ	ε	P_3/P_4	P_4/P_1	M_3	M_4	P_3/P_4	P_4/P_1	θ_3	θ_4
2.6	28.0	22.06	0.999	7.446	0.952	0.604	1.397	0.478	41.0	79.3**
2.6	29.0	25.12	1.000	7.309	0.932	0.650	1.319	0.487	44.6	76.8
2.6	30.0	28.76	1.000	7.001	0.926	0.746	1.203	0.508	52.2	72.4
2.7	1.0	-29.51	1.000	7.590	0.811	0.738	1.073	0.468	68.8	107.3
2.7	2.0	-28.49	1.000	7.707	0.847	0.704	1.148	0.461	66.4	105.8
2.7	3.0	-27.31	1.000	7.809	0.881	0.674	1.223	0.455	64.1	104.4
2.7	4.0	-25.98	1.000	7.898	0.914	0.646	1.298	0.449	61.8	103.2
2.7	5.0	-24.53	0.997	7.974	0.952	0.622	1.375	0.445	59.3	101.9**
2.7	6.0	-23.00	1.000	8.039	0.976	0.601	1.443	0.441	57.3	100.8**
2.7	7.0	-21.37	1.000	8.095	1.003	0.583	1.510	0.438	55.2	99.7**
2.7	8.0	-19.69	1.000	8.143	1.028	0.566	1.574	0.435	53.2	98.7**
2.7	9.0	-17.96	1.000	8.183	1.050	0.552	1.633	0.432	51.3	97.8**
2.7	10.0	-16.18	1.000	8.217	1.069	0.540	1.685	0.430	49.5	96.9**
2.7	11.0	-14.38	1.000	8.246	1.085	0.530	1.732	0.429	47.8	96.0**
2.7	12.0	-12.55	1.000	8.270	1.099	0.521	1.772	0.427	46.1	95.1**
2.7	13.0	-10.69	0.999	8.290	1.110	0.514	1.805	0.426	44.5	94.3**
2.7	14.0	- 8.83	1.000	8.306	1.118	0.508	1.831	0.425	43.1	93.5**
2.7	15.0	- 6.95	1.000	8.319	1.123	0.503	1.848	0.425	41.8	92.8**
2.7	16.0	- 5.05	1.000	8.328	1.126	0.500	1.859	0.424	40.5	92.0**
2.7	17.0	- 3.13	1.000	8.334	1.126	0.497	1.863	0.424	39.3	91.2**
2.7	18.0	- 1.20	1.000	8.338	1.124	0.496	1.859	0.424	38.3	90.5**
2.7	19.0	0.75	1.000	8.338	1.120	0.496	1.849	0.424	37.3	89.7**
2.7	20.0	2.72	1.000	8.335	1.113	0.497	1.832	0.424	36.5	88.9**
2.7	21.0	4.72	1.000	8.329	1.104	0.499	1.809	0.424	35.8	88.1**
2.7	22.0	6.74	1.000	8.320	1.092	0.503	1.780	0.425	35.2	87.3**
2.7	23.0	8.82	1.000	8.306	1.080	0.508	1.746	0.425	34.8	86.5**
2.7	24.0	10.94	0.999	8.288	1.065	0.515	1.706	0.426	34.6	85.6**
2.7	25.0	13.11	1.000	8.263	1.047	0.524	1.661	0.428	34.7	84.6**
2.7	26.0	15.37	1.000	8.231	1.029	0.535	1.611	0.430	35.0	83.5**
2.7	27.0	17.73	1.000	8.188	1.099	0.551	1.556	0.432	35.7	82.4**
2.7	28.0	20.24	1.000	8.128	0.987	0.571	1.494	0.436	36.9	81.0**
2.7	29.0	22.96	1.000	8.041	0.964	0.601	1.423	0.441	39.0	79.2**
2.7	30.0	26.02	1.002	7.895	0.940	0.647	1.337	0.449	42.8	76.8
2.7	31.0	29.70	1.000	7.564	0.932	0.746	1.211	0.470	50.5	72.4
2.8	1.0	-30.52	1.000	8.155	0.823	0.744	1.080	0.434	68.5	107.5
2.8	2.0	-29.49	1.000	8.287	0.861	0.708	1.162	0.426	66.0	106.0
2.8	3.0	-28.29	1.000	8.401	0.899	0.675	1.245	0.420	63.5	104.6
2.8	4.0	-26.94	1.003	8.499	0.930	0.646	1.325	0.415	61.4	103.3
2.8	5.0	-25.46	1.000	8.583	0.971	0.621	1.411	0.410	58.8	102.0**
2.8	6.0	-23.89	1.000	8.654	1.003	0.599	1.491	0.406	56.6	100.9**
2.8	7.0	-22.24	1.000	8.715	1.033	0.579	1.568	0.403	54.4	99.8**
2.8	8.0	-20.53	1.000	8.766	1.060	0.563	1.640	0.400	52.4	98.8**
2.8	9.0	-18.77	1.000	8.810	1.084	0.548	1.707	0.398	50.4	97.8**
2.8	10.0	-16.97	1.000	8.846	1.105	0.536	1.767	0.396	48.5	96.9**
2.8	11.0	-15.14	0.999	8.878	1.124	0.525	1.822	0.395	46.7	96.1**
2.8	12.0	-13.30	1.000	8.903	1.138	0.516	1.867	0.393	45.0	95.3**
2.8	13.0	-11.44	1.000	8.925	1.150	0.508	1.906	0.392	43.4	94.5**
2.8	14.0	- 9.57	1.000	8.942	1.159	0.502	1.936	0.391	41.9	93.7**
2.8	15.0	- 7.69	1.000	8.956	1.165	0.497	1.957	0.391	40.5	92.9**
2.8	16.0	- 5.80	1.000	8.967	1.168	0.493	1.970	0.390	39.2	92.2**
2.8	17.0	- 3.89	1.000	8.974	1.169	0.490	1.975	0.390	38.0	91.5**

TABLE 1—concluded

M_1	δ	ε	p_3/p_4	p_4/p_1	M_3	M_4	P_3/P_4	P_4/P_1	θ_3	θ_4
2.8	18.0	— 1.98	1.000	8.978	1.167	0.489	1.972	0.390	36.9	90.7**
2.8	19.0	— 0.05	1.000	8.980	1.162	0.488	1.962	0.389	35.8	90.0**
2.8	20.0	1.90	1.000	8.979	1.156	0.489	1.944	0.390	34.9	89.3**
2.8	21.0	3.86	1.000	8.974	1.146	0.490	1.920	0.390	34.2	88.5**
2.8	22.0	5.85	1.000	8.966	1.135	0.493	1.889	0.390	33.5	87.8**
2.8	23.0	7.87	1.000	8.955	1.121	0.497	1.852	0.391	33.0	87.0**
2.8	24.0	9.94	1.000	8.939	1.106	0.503	1.810	0.392	32.7	86.2**
2.8	25.0	12.04	1.000	8.918	1.089	0.511	1.762	0.393	32.5	85.3**
2.8	26.0	14.22	0.999	8.891	1.070	0.520	1.709	0.394	32.6	84.3**
2.8	27.0	16.46	1.000	8.856	1.048	0.532	1.652	0.396	33.0	83.3**
2.8	28.0	18.82	1.000	8.808	1.025	0.549	1.589	0.398	33.8	82.1**
2.8	29.0	21.33	1.000	8.743	1.000	0.570	1.519	0.402	35.1	80.7**
2.8	30.0	24.06	1.000	8.647	0.974	0.601	1.440	0.407	37.3	79.0**
2.8	31.0	27.15	1.003	8.485	0.946	0.650	1.344	0.415	41.5	76.5
2.8	32.0	30.96	1.000	8.083	0.938	0.764	1.198	0.438	50.3	71.7



(a) Wedge intake of sub-critical mass flow ratio



(b) Shock wave-boundary layer interaction

FIG. 1. Two examples of flows involving the intersection of a weak shock wave and a strong shock.

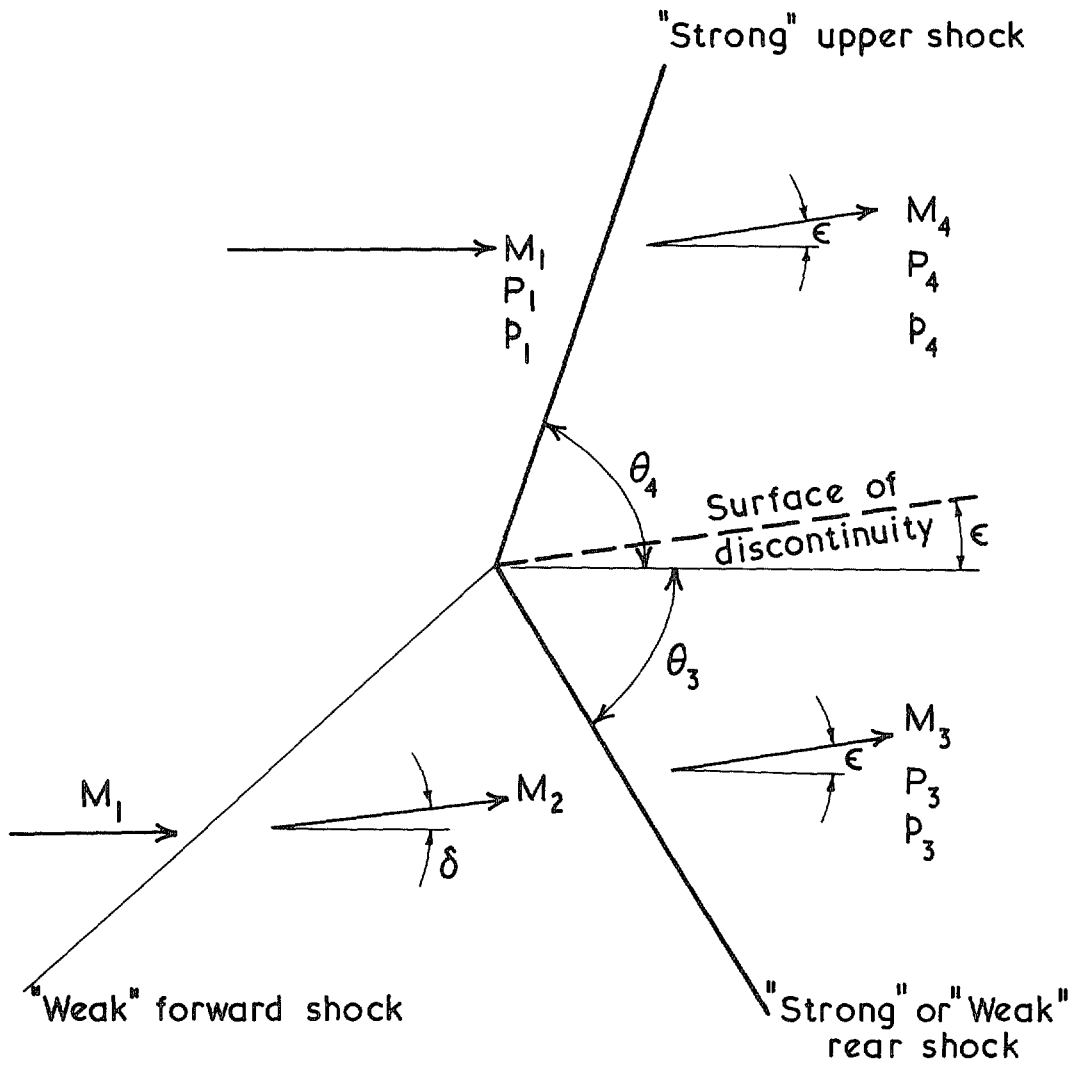


FIG. 2. Definitions and notation.

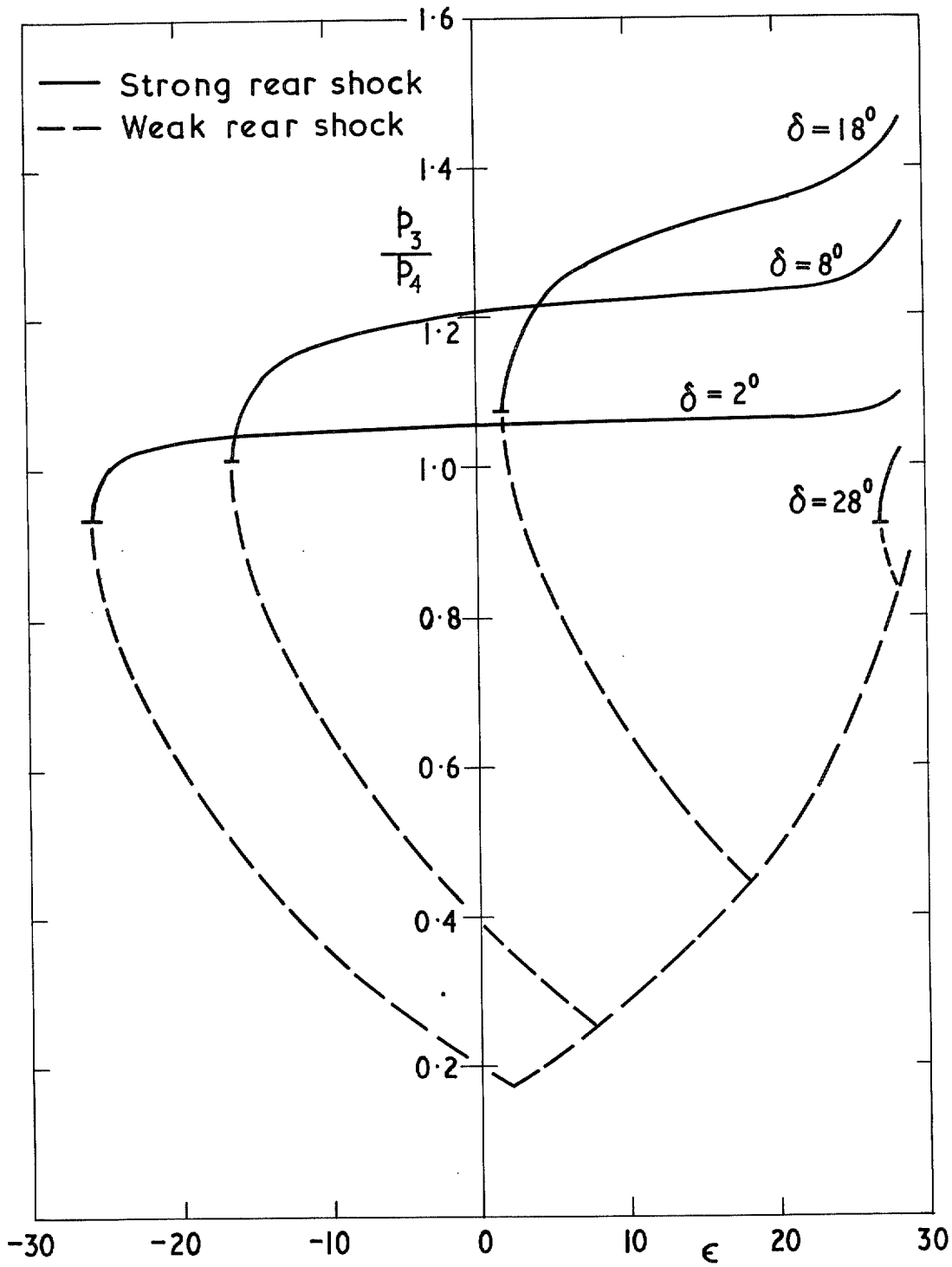


FIG. 3. Static pressure ratio across lamina replacing vortex sheet, $M_1 = 2.4$.

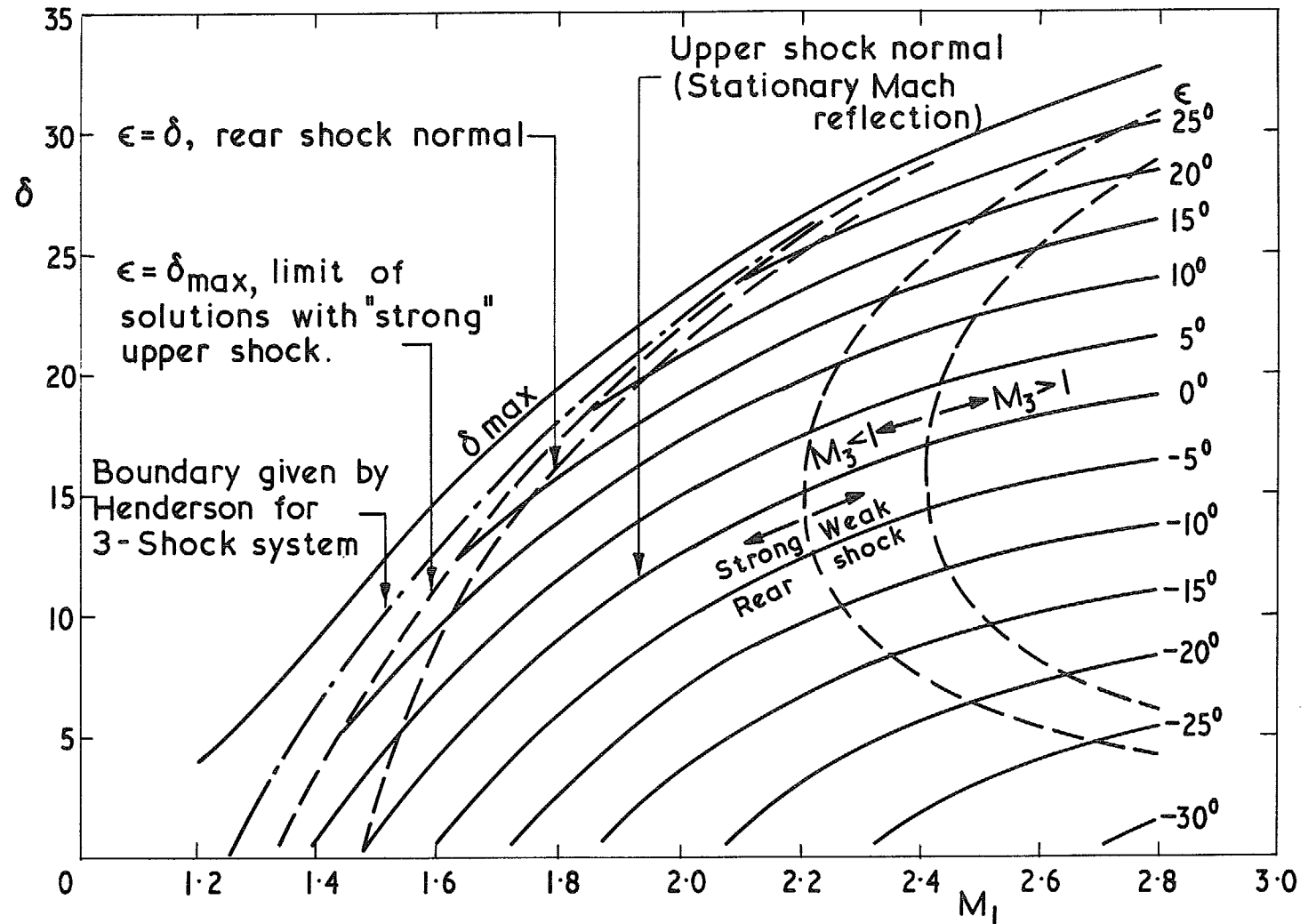
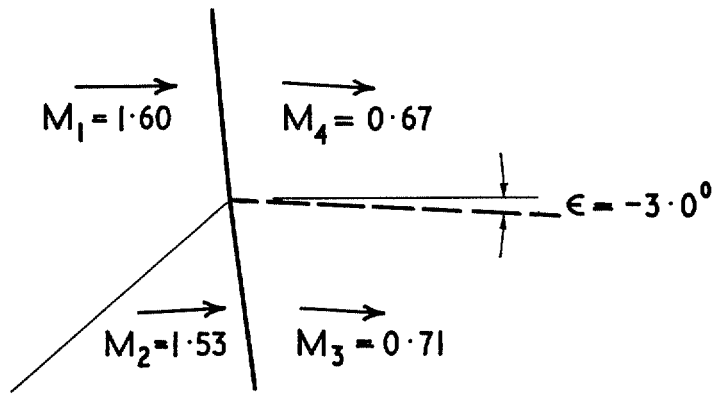
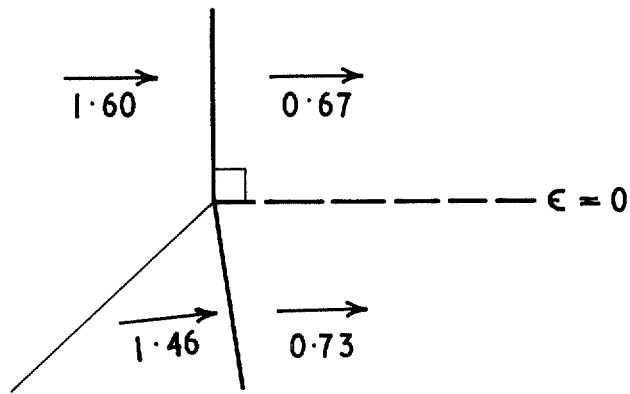


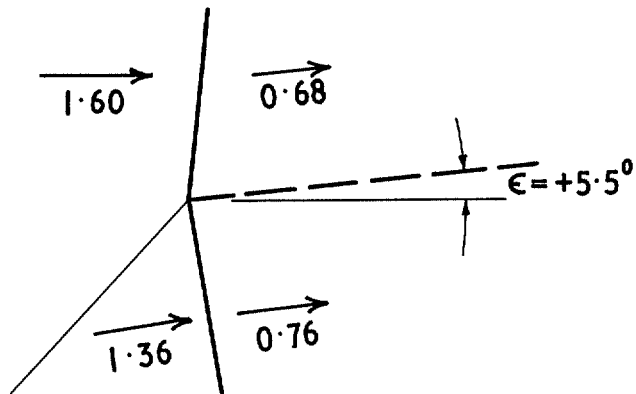
FIG. 4. Summary of results for the intersection of a weak shock wave with a strong shock.



(a) $\delta = 2^\circ$, ϵ is negative

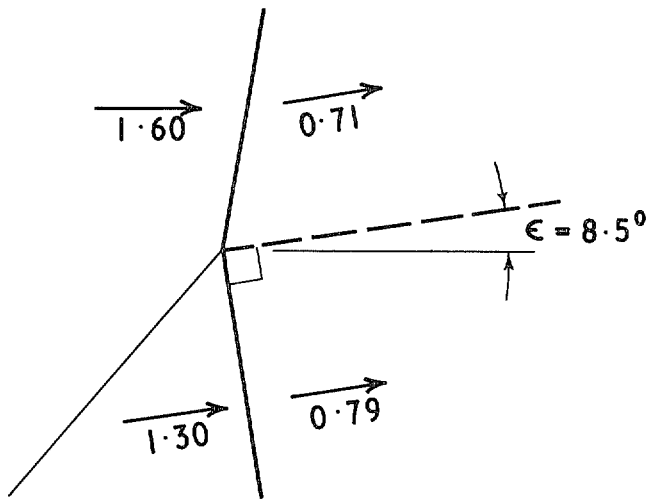


(b) $\delta \simeq 4^\circ$, $\epsilon = 0$, Upper shock normal

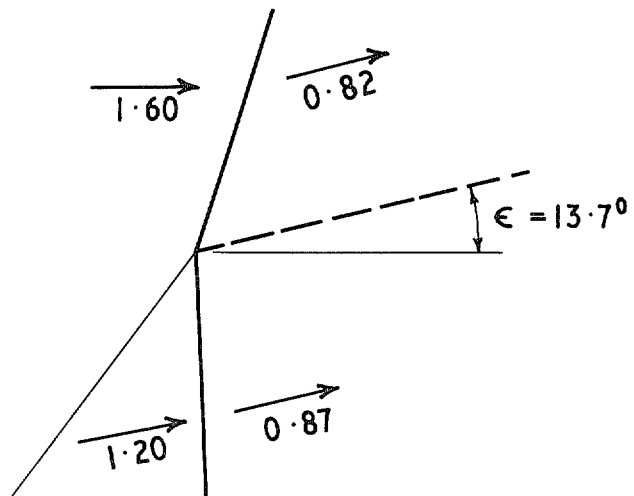


(c) $\delta = 7^\circ$, $\epsilon < \delta$

FIG. 5. Changes in shock intersection patterns with increasing flow deflection through the forward shock wave, $M_1 = 1.6$.



(d) $\delta = \epsilon \approx 8.5^\circ$, Rear shock normal



(e) $\delta = 11^\circ$, $\epsilon > \delta$.

FIG. 5. (cont'd.)

© Crown copyright 1973

HER MAJESTY'S STATIONERY OFFICE

Government Bookshops

49 High Holborn, London WC1V 6HB
13a Castle Street, Edinburgh EH2 3AR
109 St Mary Street, Cardiff CF1 1JW
Brazenose Street, Manchester M60 8AS
50 Fairfax Street, Bristol BS1 3DE
258 Broad Street, Birmingham B1 2HE
80 Chichester Street, Belfast BT1 4JY

*Government publications are also available
through booksellers*